# Supplementary Information for

# Measurement report: Surface exchange fluxes of HONO during the growth process of paddy fields in the Huaihe River Basin, China

Fanhao Meng[1,3,a], Baobin Han[1,2,a], Min Qin[1], Wu Fang[1], Ke Tang[4], Dou Shao[1,2], Zhitang Liao[1,2], Jun Duan[1], Yan Feng[5,6], Yong Huang[5,6], Ting Ni[5,6], Pinhua Xie[1,2,7]

[1] Key Laboratory of Environmental Optics and Technology, Anhui Institute of Optics and Fine Mechanics, Hefei Institutes of Physical Science, Chinese Academy of Sciences, Hefei, 230031, China

[2] University of Science and Technology of China, Hefei, 230026, China

[3] State Key Laboratory of Pulsed Power Laser Technology, National University of Defense Technology, Hefei 230037, China

[4] School of Electrical and Photoelectronic Engineering, West Anhui University, Luan 237012, China

[5] Anhui Institute of Meteorological Sciences, Anhui Province Key Laboratory of Atmospheric Science and Satellite Remote Sensing, Hefei 230031, China

[6] Shouxian National Climatology Observatory, Huaihe River Basin Typical Farm Eco-meteorological Experiment Field of CMA, Shouxian 232200, China

[7] CAS Center for Excellence in Regional Atmospheric Environment, Institute of Urban Environment, Chinese Academy of Sciences, Xiamen, 361021, China

[a] These authors contributed equally to this work.

*Correspondence to*: Min Qin (mqin@aiofm.ac.cn)

**Text S1 Meteorological and micrometeorological measurements**

The meteorological data including wind speed, wind direction, air temperature ($T_{air}$), and relative humidity (RH) were recorded by an automatic weather station (HydroMetTM, Vaisala, Finland). Precipitation and solar radiation were measured with a TR-YL rain gauge (Veinasa, China) and baseline surface radiation station (BSRN3000, TRUWEL Instrument Inc., China). Soil parameters including soil temperature ($T_{soil}$) (TMC6-HC, ONSET, USA) and soil water content ($\theta$) (S-SMD-M005, ONSET, USA) were measured at a depth of 5 cm. The photolysis frequency of HONO ($J$(HONO)) and $NO_2$ ($J(NO_2)$) was calculated from global radiation according to Trebs et al. (2009). The Tropospheric Ultraviolet and Visible (TUV) radiation model was also used to calculate UV spectral irradiance and photolysis frequency for cloudless days, and the simulated photolysis frequency ($J(O^1D)$) was corrected by adopting the observed UV intensity (Liu et al., 2019a). The particle matter concentration and number size distribution were continuously measured with Grimm EDM180. The aerosol surface density ($S_a$) was derived from the particle number size distributions of 0.25-32 μm.

Eddy covariance measurements were performed with an integrated 3-D ultrasonic anemometer and open-path $CO_2/H_2O$ analyzer (IRGASON, Campbell Sci. Inc., USA) mounted at 4 m height, with data collected and recorded at 10 Hz. The friction velocity ($u_*$) and the Obukhov length ($L$) were calculated with Edire software (Robert Clement, University of Edinburgh, UK). The footprint analysis was performed with the ART Footprint Tool described by (Neftel et al., 2008), which indicated that >82 % of the field was in the mast footprint on average.

**Text S2 Chemical reactions in the turbulent transport**

The chemical reactions for reactive trace gases (HONO, NO, and $NO_2$) need to be considered in determining HONO, NO, and $NO_2$ fluxes since the AG method is strictly valid only for non-reactive trace gases. The comparison of turbulent transport and chemical reaction timescales demonstrated whether chemical reactions could occur in the transport of chemical species, and thus whether these can be regarded as passive scalar (Stella et al., 2012). The ratio of turbulent transport timescale ($\tau_{\mathrm{trans}}$) and chemical reaction timescale ($\tau_{\mathrm{chem}}$) is defined as Damköhler number ($DA$) ($DA=\tau_{\mathrm{trans}}/\tau_{\mathrm{chem}}$), which identifies flux divergence from the chemical reactions (Laufs et al., 2017; Meng et al., 2022; Stella et al., 2012). The turbulent transport time was estimated between the reference height ($z_{ref}$) and the ground surface (or canopy exchange height), which was simply expressed as the product of transfer resistance and layer height (Garland, 1997):

$$\tau_{\mathrm{trans}} = R_{\mathrm{a}}(z) \cdot (z_{\mathrm{ref}} - d - z_0) + R_{\mathrm{b}} \cdot (z_0 - z_{0'})$$

$$\approx R_{\mathrm{a}}(\mathrm{z}) \cdot (z_{\mathrm{ref}} - d - z_0) \quad \text{(S1)}$$

$$R_{\mathrm{a}}(\mathrm{z}) = \frac{u(z)}{u_*^2} - \frac{\Psi_{\mathrm{H}}(z/L) - \Psi_{\mathrm{M}}(z/L)}{\kappa u_*} \quad \text{(S2)}$$

where $R_{\mathrm{a}}(z)$ and $R_{\mathrm{b}}$ are the aerodynamic resistance and quasi-laminar boundary layer resistance, where $R_{\mathrm{b}}$ was small and could be neglected; $z_0$ and $z_{0'}$ are the roughness height for the momentum and the scalar, respectively; $\Psi_{\mathrm{M}}$ is integrated stablity corection fuction for momentum (Sutton et al., 1993). The chemical reaction time of HONO and NO-$O_3$-$NO_2$ triad gives characteristic timescale in turbulent transport.

$$\mathrm{NO} + \mathrm{O_3} \rightarrow \mathrm{NO_2} + \mathrm{O_2} \quad \text{(R1)}$$

$$\mathrm{NO_2} + \mathrm{O_2} + h\nu(\lambda \leq 400\mathrm{nm}) \rightarrow \mathrm{NO} + \mathrm{O_3} \quad \text{(R2)}$$

$$\mathrm{HONO} + h\nu(320\mathrm{nm} < \lambda < 405\mathrm{nm}) \rightarrow \mathrm{NO} + \mathrm{OH} \quad \text{(R3)}$$

The reactions of NO + OH and HONO + OH, which are much less than HONO photolysis, were not considered in calculation of HONO chemical time. The reaction (R3) for the reaction of the NO-$O_3$-$NO_2$ triad could also be neglected (Stella et al., 2012). Thus, the chemical reaction timescale for HONO and NO-$O_3$-$NO_2$ triad were estimated as follows:

$$\tau_{\mathrm{chem}} = \frac{1}{J(\mathrm{HONO})} \quad \text{(S3)}$$

$$\tau_{\mathrm{chem}} = \frac{2}{\sqrt{J(\mathrm{NO_2})^2 + k^2(\overline{[\mathrm{O_3}]} - \overline{[\mathrm{NO}]}^2) + 2J(\mathrm{NO_2})k(\overline{[\mathrm{O_3}]} + \overline{[\mathrm{NO}]} + 2\overline{[\mathrm{NO_2}]})}} \quad \text{(S4)}$$

where $k$ is the rate coefficient (Walton et al., 1997), $\overline{[\mathrm{NO}]}$, $\overline{[\mathrm{NO_2}]}$ and $\overline{[\mathrm{O_3}]}$ are the mixing ratios at the measurement height. The daytime transfer time was typically less than 1 min, which was much smaller than the HONO chemical lifetime ($\tau_{\mathrm{chem}}$ ≥9 min). The influence of HONO flux photolytic loss was always below 10 % (*DA*<0.1), which gave an upper limit for the flux divergence and could be neglected for further analysis. For the chemical reactions of NO-$O_3$-$NO_2$ triad, the small chemical timescale induced a flux divergence that was dependent on the Damköhler number in turbulent transport. However, the fluxes with chemical corrections were not available due to the lack of $O_3$ flux measurement (Lenschow and Delany, 1987). The typical *DA* was smaller than 1 with flux divergence between 0 % and 25 % (Stella et al., 2012). Therefore, the fluxes without chemical corrections were lower than the actual NO and $NO_2$ fluxes.

**Text S3 Calculation of HONO sources and sinks**

**HONO sources**

***Homogeneous reaction***

The HONO production from the homogeneous reaction of NO and OH is calculated as follows:

$$P_{\mathrm{OH+NO}} = k_{\mathrm{OH+NO}}[\mathrm{OH}][\mathrm{NO}] \quad \text{(S5)}$$

The rate constant of $k_{\mathrm{OH+NO}}$ is $9.8\times10^{-12}$ $\mathrm{cm^3}$ $\mathrm{molecules^{-1}}$ $\mathrm{s^{-1}}$ (Atkinson et al., 2004), and $[\mathrm{OH}]$ and $[\mathrm{NO}]$ are the mixing ratios of OH (molecules $\mathrm{cm^{-3}}$) and NO (ppbv), respectively. The OH concentrations are derived by applying the empirical equation (Liu et al., 2019a):

$$[\mathrm{OH}] = a \times (J(\mathrm{O^1D})/10^{-5})^b + c \quad \text{(S6)}$$

where $a$ and $b$ characterize the influence of the reactants and photolytic processes on OH, with coefficients $a$=$4.2\times10^6$ molecules $\mathrm{cm^{-3}}$ and $b$=1, respectively. The coefficient c counts light-independent OH sources, which is $1\times10^6$ $\mathrm{cm^{-3}}$ in summer.

***Heterogeneous conversion of $NO_2$ on the surfaces***

The heterogeneous conversion of $NO_2$ on the surface is considered as a significant source of HONO. The reaction (R4) assumes that HONO and $HNO_3$ are formed by equimolar disproportionation of two $NO_2$ molecules and immediately release HONO (Finlayson-Pitts et al., 2003; Finlayson-Pitts, 2009). The HONO production from the heterogeneous reaction of $NO_2$ on the aerosol surface and the ground surface can be calculated as follows:

$$2\mathrm{NO_2} + \mathrm{H_2O} \rightarrow \mathrm{HONO} + \mathrm{HNO_3} \quad \text{(R4)}$$

$$P_{\mathrm{aerosol}} = \frac{v(\mathrm{NO_2})\times\gamma_a\times S_a\times[\mathrm{NO_2}]}{8} \quad \text{(S7)}$$

$$P_{\mathrm{ground}} = \frac{v(\mathrm{NO_2})\times\gamma_g\times[\mathrm{NO_2}]}{8\times MLH} \quad \text{(S8)}$$

where $v(\mathrm{NO_2})$ is the molecule speed of $NO_2$ (m $\mathrm{s^{-1}}$), $v(\mathrm{NO_2}) = \sqrt{\frac{8RT}{\pi M}}$; $S_a$ is the aerosol surface areas ($\mathrm{m^{-1}}$) derived from the aerosol size distribution, $[\mathrm{NO_2}]$ is the $NO_2$ concentration (ppbv), $\gamma_a$ and $\gamma_g$ is the uptake coefficient of $NO_2$ on the aerosol surface and the ground surface, which is supposed to be $1\times10^{-6}$ (Hu et al., 2023).

The vertical mixing process is determined by the turbulence, and the vertical transmission distance of HONO ($\Delta z$) over time $\tau$ could be considered as the upper limit of MLH, which can be calculated as follow (Xue et al., 2021):

$$\Delta z = \sqrt{2 \times K_z \times \tau} \quad \text{(S9)}$$

where $K_z$ is the turbulent diffusion coefficient, with a typical value of $3\times10^5$ $\mathrm{cm^2}$ $\mathrm{s^{-1}}$, and $\tau$ is the photolytic lifetime of HONO. The calculated $\Delta z$ is 205 m at 12:00, coinciding with the shortest

photolytic lifetime of HONO (699 s, $J(\mathrm{HONO})$=1.4×10$^{-3}$ s$^{-1}$). Since MLH is expected to exhibit a similar variability to the boundary layer height (BLH), the diurnal profile of MLH is determined by utilizing the diurnal BLH data sourced from ECMWF (European Center for Medium-Range Weather Forecasts) and scaled by the ratio of $\Delta z$-to-BLH at 12:00, the calculated MLH is shown in Fig. S5.

***Soil emission***

The emission rate of HONO from soil was calculated based on the emission flux and the mixing layer height according to the following equation:

$$P_{\mathrm{soil}} = \frac{10^9 \times 3600 \times R \times T \times F_{\mathrm{HONO}}}{M \times P \times MLH} \quad \text{(S10)}$$

where $F_{\mathrm{HONO}}$ is the HONO flux (ng m$^{-2}$ s$^{-1}$), $R$ is the ideal gas constant (J mol$^{-1}$ K$^{-1}$), $T$ is the temperature (K), $M$ is the molecular weight (g mol$^{-1}$), $P$ is the atmospheric pressure (Pa), $MLH$ is mixing layer height (m).

***Photosensitized conversion of $NO_2$ on the surfaces***

The heterogeneous conversion of $NO_2$ on the aerosol surface and the ground surface can be parameterized as follows:

$$\mathrm{NO_2} + h\nu \xrightarrow{\text{surface}} \mathrm{HONO} \quad \text{(R5)}$$

$$P_{\mathrm{aerosol}+h\nu} = \frac{v(\mathrm{NO_2}) \times \gamma_{a+h\nu} \times S_a \times [\mathrm{NO_2}]}{4} \times \frac{J(\mathrm{NO_2})}{J(\mathrm{NO_2})_{noon}} \quad \text{(S11)}$$

$$P_{\mathrm{ground}+h\nu} = \frac{v(\mathrm{NO_2}) \times \gamma_{g+h\nu} \times [\mathrm{NO_2}]}{4 \times MLH} \times \frac{J(\mathrm{NO_2})}{J(\mathrm{NO_2})_{noon}} \quad \text{(S12)}$$

where $\gamma_{a+h\nu}$ and $\gamma_{g+h\nu}$ are the photo-enhanced uptake coefficient of $NO_2$ on the aerosol surface and the ground surface, respectively. $\frac{J(\mathrm{NO_2})}{J(\mathrm{NO_2})_{noon}}$ is photo-enhanced factor, and $J(\mathrm{NO_2})_{noon}$ is set to 0.005 s$^{-1}$ (Liu et al., 2019b; Wong et al., 2013). The photo-enhanced uptake coefficient of 10$^{-6}$ to 10$^{-4}$ was derived from previous studies, which is supposed to be 1×10$^{-5}$ (Chen et al., 2023; Han et al., 2016; Monge et al., 2010; Song et al., 2022; Wong et al., 2013).

**HONO sinks**

The sinks of HONO contain the photolysis ($L_{\mathrm{photo}}$), the reaction of HONO with OH ($L_{\mathrm{OH+HONO}}$) and dry deposition loss ($L_{\mathrm{dep}}$), which can be calculated by the following formulas:

$$L_{\mathrm{photo}} = J(\mathrm{HONO})[\mathrm{HONO}] \quad \text{(S13)}$$

$$L_{\mathrm{OH+HONO}} = k_{\mathrm{OH+HONO}}[\mathrm{OH}][\mathrm{HONO}] \quad \text{(S14)}$$

$$L_{\mathrm{dep}} = \frac{v(\mathrm{HONO})}{MLH}[\mathrm{HONO}] \quad \text{(S15)}$$

where $J$(HONO) is photolysis frequency of HONO ($s^{-1}$), $k_{OH+HONO}$ is $6\times10^{-12}$ $cm^3$ $molecules^{-1}$ $s^{-1}$, which is rate constant (Atkinson et al., 2004); $v$(HONO) is deposition velocity of HONO, which is supposed to be 0.0048 m $s^{-1}$ (Lee et al., 2016; Zhang et al., 2023).

**Text S4 Calculation of OH production**

The net OH production rate, $P_{OH}(HONO)_{net}$, was calculated by OH production from HONO photolysis ($P_{OH}$(HONO)) subtracting the OH loss terms (OH+HONO and OH+NO) (Eqs. (S16)). The OH production rate from $O_3$ photolysis was calculated by Eq. (S17) (Li et al., 2018; Su et al., 2008).

$$P_{OH}(HONO)_{net} = J_{HONO}[HONO] - k_{OH+NO}[OH][NO] - k_{OH+HONO}[OH][HONO] \quad (S16)$$

$$P_{OH}(O_3) = 2J(O^1D)[O_3]/(1 + k_3[M]/k_2[H_2O]) \quad (S17)$$

where $k_2$=$2.2\times10^{-10}$ $cm^3$ $molecules^{-1}$ $s^{-1}$ and $k_3$=$2.6\times10^{-11}$ $cm^3$ $molecules^{-1}$ $s^{-1}$ are the reaction rate constants of the $O^1D$ branch reaction, respectively.

**Figures**

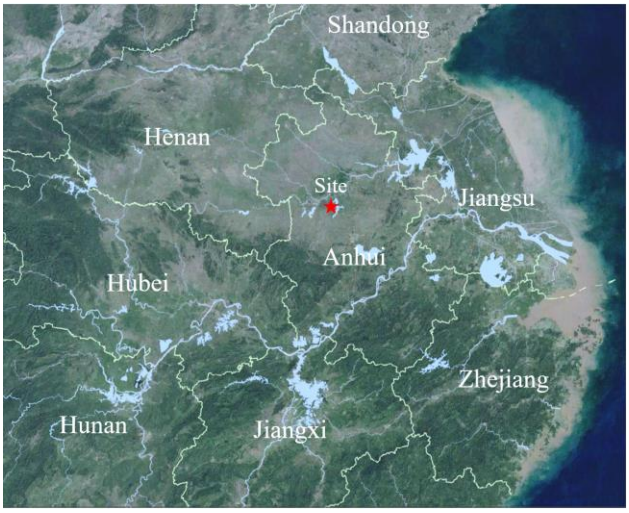


**Figure S1.** Location of the Shouxian National Climatological Observatory (red star, 32°25′ N, 116°47′ E). The map is adapted from ©Google Earth.

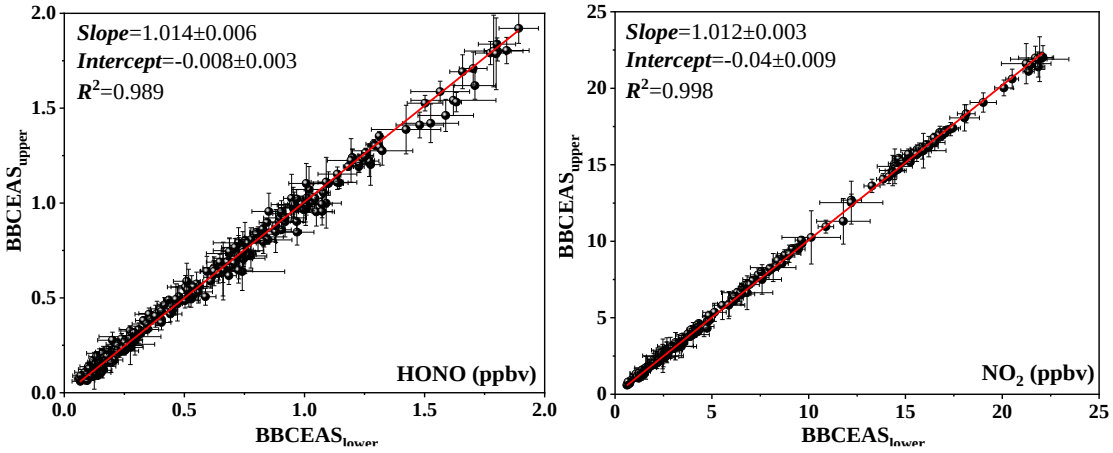


**Figure S2.** Intercomparison of HONO and $NO_2$ mixing ratios measured by $BBCEAS_{lower}$ at 0.2/0.3 m level and $BBCEAS_{upper}$ at 1.6 m level, where the slope and intercept with $2\sigma$ standard deviation are given.

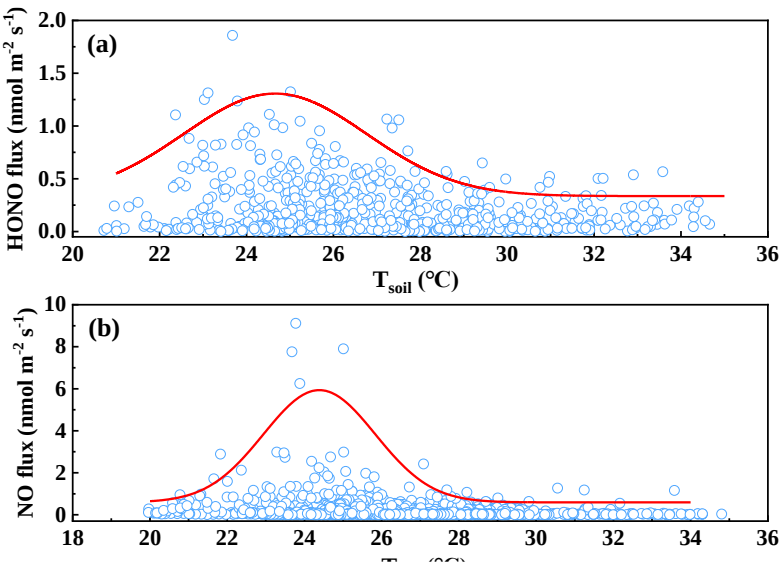


**Figure S3.** Emissions of (a) HONO and (b) NO as a function of soil temperature over the rotary tillage. The curves are gaussian fitting the fluxes of HONO and NO with soil temperature.

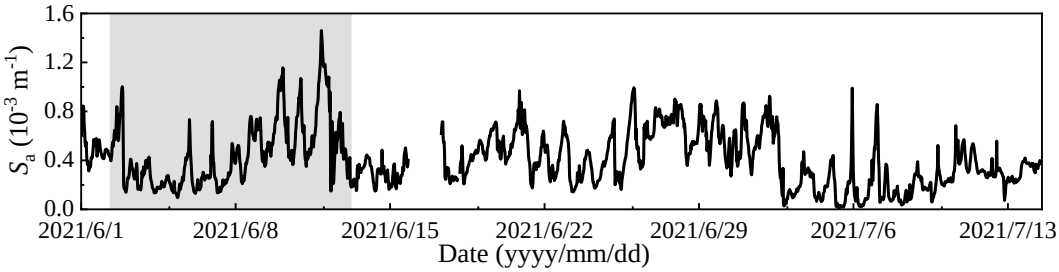


**Figure S4.** Time series of aerosol surface area ($S_a$) during the whole campaign. The shaded area represents the rotary tillage period.

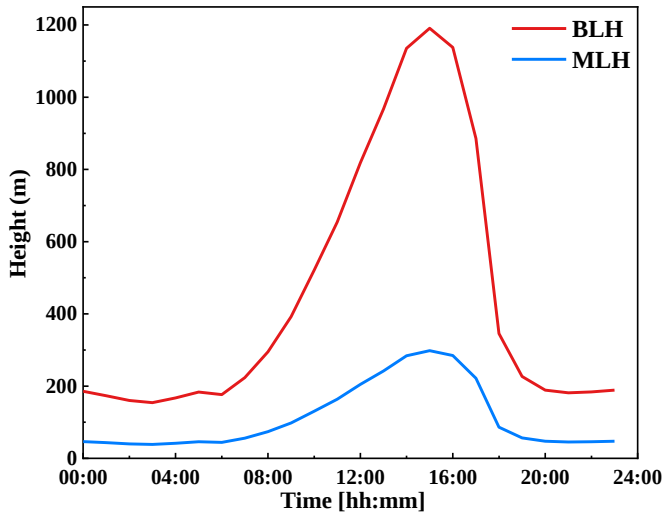


**Figure S5.** The diurnal variation of BLH was obtained from ECMWF and the calculated MLH.

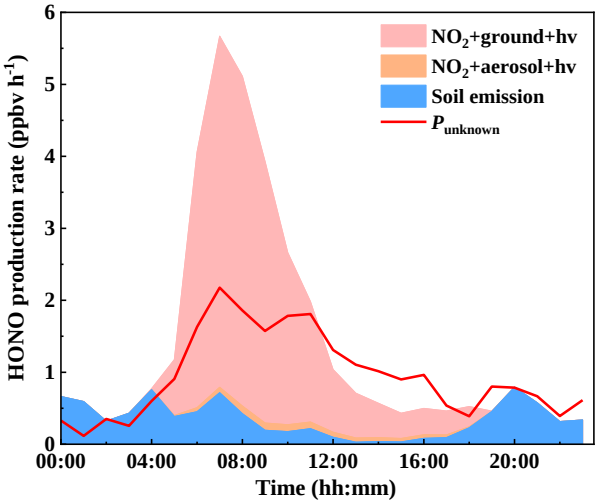


**Figure S6.** Diurnal variation of photosensitive conversion of $NO_2$ on the surfaces and HONO flux rates derived from soil emissions. The upper limit of photo-enhanced uptake coefficient of $3.5\times10^{-5}$ was utilized to estimate the $P_{\text{aerosol}+h\nu}$ and $P_{\text{ground}+h\nu}$.

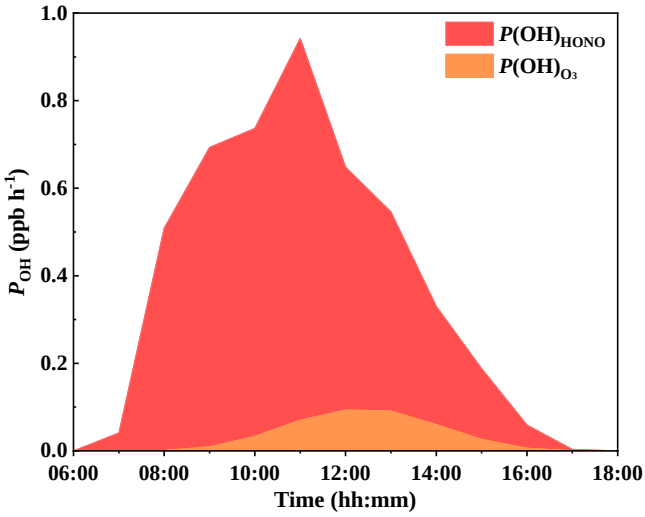


**Figure S7.** Diurnal variation of net OH production rate of the photolysis of HONO ($P(\text{OH})_{\text{HONO}}$) and $O_3$ ($P(\text{OH})_{O_3}$) over the winter campaign.

## References


Atkinson, R., Baulch, D. L., Cox, R. A., Crowley, J. N., Hampson, R. F., Hynes, R. G., Jenkin, M. E., Rossi, M. J., and Troe, J.: Evaluated kinetic and photochemical data for atmospheric chemistry: Volume I -: gas phase reactions of $O_x$, $HO_x$, $NO_x$ and $SO_x$ species, Atmos. Chem. Phys., 4, 1461-1738, https://doi.org/10.5194/acp-4-1461-2004, 2004.

Chen, D., Zhou, L., Liu, S., Lian, C., Wang, W., Liu, H., Li, C., Liu, Y., Luo, L., Xiao, K., Chen, Y., Qiu, Y., Tan, Q., Ge, M., and Yang, F.: Primary sources of HONO vary during the daytime: Insights based on a field campaign, Sci. Total Environ., 903, 16605, https://doi.org/10.1016/j.scitotenv.2023.166605, 2023.

Finlayson-Pitts, B. J.: Reactions at surfaces in the atmosphere: integration of experiments and theory as necessary (but not necessarily sufficient) for predicting the physical chemistry of aerosols, Phys. Chem. Chem. Phys., 11, 7760-7779, https://doi.org/10.1016/10.1039/b906540g, 2009.

Finlayson-Pitts, B. J., Wingen, L. M., Sumner, A. L., Syomin, D., and Ramazan, K. A.: The heterogeneous hydrolysis of $NO_2$ in laboratory systems and in outdoor and indoor atmospheres: An integrated mechanism, Phys. Chem. Chem. Phys., 5, 223-242, https://doi.org/10.1039/b208564j, 2003.

Garland, J. A.: The dry deposition of sulphur dioxide to land and water surfaces, P. Roy. Soc. A-Math. Phy., 354, 245-268, https://doi.org/10.1098/rspa.1977.0066, 1997.

Han, C., Yang, W., Wu, Q., Yang, H., and Xue, X.: Heterogeneous Photochemical Conversion of $NO_2$ to HONO on the Humic Acid Surface under Simulated Sunlight, Environ. Sci. Technol., 50, 5017-5023, https://doi.org/10.1021/acs.est.5b05101, 2016.

Hu, B., Chen, G., Chen, J., Xu, L., Fan, X., Hong, Y., Li, M., Lin, Z., Huang, M., Zhang, F., and Wang, H.: The effect of nitrous acid (HONO) on ozone formation during pollution episodes in southeastern China: Results from model improvement and mechanism insights, Sci. Total Environ., 891, 164477, https://doi.org/10.1016/j.scitotenv.2023.164477, 2023.

Laufs, S., Cazaunau, M., Stella, P., Kurtenbach, R., Cellier, P., Mellouki, A., Loubet, B., and Kleffmann, J.: Diurnal fluxes of HONO above a crop rotation, Atmos. Chem. Phys., 17, 6907-6923, https://doi.org/10.5194/acp-17-6907-2017, 2017.

Lee, J. D., Whalley, L. K., Heard, D. E., Stone, D., Dunmore, R. E., Hamilton, J. F., Young, D. E., Allan, J. D., Laufs, S., and Kleffmann, J.: Detailed budget analysis of HONO in central London reveals a missing daytime source, Atmos. Chem. Phys., 16, 2747-2764, https://doi.org/10.5194/acp-16-2747-2016, 2016.

Lenschow, D. H. and Delany, A. C.: An analytic formulation for NO and $NO_2$ flux profiles in the atmospheric surface layer, J. Atmos. Chem., 5, 301-309, https://doi.org/10.1007/BF00114108, 1987.

Li, D., Xue, L., Wen, L., Wang, X., Chen, T., Mellouki, A., Chen, J., and Wang, W.: Characteristics and sources of nitrous acid in an urban atmosphere of northern China: Results from 1-yr continuous observations, Atmos. Environ., 182, 296-306, https://doi.org/10.1016/j.atmosenv.2018.03.033, 2018.

Liu, Y., Nie, W., Xu, Z., Wang, T., Wang, R., Li, Y., Wang, L., Chi, X., and Ding, A.: Semi-quantitative understanding of source contribution to nitrous acid (HONO) based on 1 year of continuous observation at the SORPES station in eastern China, Atmos. Chem. Phys., 19, 13289-13308, https://doi.org/10.5194/acp-19-13289-2019, 2019a.

Liu, Y., Lu, K., Li, X., Dong, H., Tan, Z., Wang, H., Zou, Q., Wu, Y., Zeng, L., Hu, M., Min, K. E., Kecorius, S., Wiedensohler, A., and Zhang, Y.: A Comprehensive Model Test of the HONO Sources Constrained to Field Measurements at Rural North China Plain, Environ. Sci. Technol., 53, 3517-3525, https://doi.org/10.1021/acs.est.8b06367, 2019b.

Meng, F., Qin, M., Fang, W., Duan, J., Tang, K., Zhang, H., Shao, D., Liao, Z., Feng, Y., Huang, Y., Ni, T., Xie, P., Liu, J., and Liu, W.: Measurement of HONO flux using the aerodynamic gradient method over an agricultural field in the Huaihe River Basin, China, J. Environ. Sci., 114, 297-307, https://doi.org/10.1016/j.jes.2021.09.005, 2022.

Monge, M. E., D'Anna, B., Mazri, L., Giroir-Fendler, A., Ammann, M., Donaldson, D. J., and George, C.: Light changes the atmospheric reactivity of soot, P. Natl. Acad. Sci. USA, 107, 6605-6609, https://doi.org/10.1073/pnas.0908341107, 2010.

Neftel, A., Spirig, C., and Ammann, C.: Application and test of a simple tool for operational footprint evaluations, Environ. Pollut., 152, 644-652, https://doi.org/10.1016/j.envpol.2007.06.062, 2008.

Song, Y., Zhang, Y., Xue, C., Liu, P., He, X., Li, X., and Mu, Y.: The seasonal variations and potential sources of nitrous acid (HONO) in the rural North China Plain, Environ. Pollut., 311, 119967, https://doi.org/10.1016/j.envpol.2022.119967, 2022.

Stella, P., Loubet, B., Laville, P., Lamaud, E., Cazaunau, M., Laufs, S., Bernard, F., Grosselin, B., Mascher, N., Kurtenbach, R., Mellouki, A., Kleffmann, J., and Cellier, P.: Comparison of methods for the determination of NO-$O_3$-$NO_2$ fluxes and chemical interactions over a bare soil, Atmos. Meas. Tech., 5, 1241-1257, https://doi.org/10.5194/amt-5-1241-2012, 2012.

Su, H., Cheng, Y. F., Shao, M., Gao, D. F., Yu, Z. Y., Zeng, L. M., Slanina, J., Zhang, Y. H., and Wiedensohler, A.: Nitrous acid (HONO) and its daytime sources at a rural site during the 2004 PRIDE-PRD experiment in China, J. Geophys. Res-Atmos., 113, D14312, https://doi.org/10.1029/2007JD009060, 2008.

Sutton, M. A., Fowler, D., and Moncrieff, J. B.: The exchange of atmospheric ammonia with vegetated surfaces. I: Unfertilized vegetation, Q. J. Roy. Meteor. Soc., 119, 1023-1045, https://doi.org/10.1016/S1352-2310(97)00164-7, 1993.

Trebs, I., Bohn, B., Ammann, C., Rummel, U., Blumthaler, M., Koenigstedt, R., Meixner, F. X., Fan, S., and Andreae, M. O.: Relationship between the $NO_2$ photolysis frequency and the solar global irradiance, Atmos. Meas. Tech., 2, 725-739, https://doi.org/10.5194/amt-2-725-2009, 2009.

Walton, S., Gallagher, M. W., and Duyzer, J. H.: Use of a detailed model to study the exchange of $NO_x$ and $O_3$ above and below a deciduous canopy, Atmos. Environ., 31, 2915-2931, https://doi.org/10.1016/S1352-2310(97)00126-X, 1997.

Wong, K. W., Tsai, C., Lefer, B., Grossberg, N., and Stutz, J.: Modeling of daytime HONO vertical gradients during SHARP 2009, Atmos. Chem. Phys., 13, 3587-3601, https://doi.org/10.5194/acp-13-3587-2013, 2013.

Xue, C., Ye, C., Zhang, C., Catoire, V., Liu, P., Gu, R., Zhang, J., Ma, Z., Zhao, X., Zhang, W., Ren, Y., Krysztofiak, G., Tong, S., Xue, L., An, J., Ge, M., Mellouki, A., and Mu, Y.: Evidence for Strong HONO Emission from Fertilized Agricultural Fields and its Remarkable Impact on Regional $O_3$ Pollution in the Summer North China Plain, ACS Earth Space Chem., 5, 340-347, https://doi.org/10.1021/acsearthspacechem.0c00314, 2021.

Zhang, S., Li, G., Ma, N., He, Y., Zhu, S., Pan, X., Dong, W., Zhang, Y., Luo, Q., Ditas, J., Kuhn, U., Zhang, Y., Yuan, B., Wang, Z., Cheng, P., Hong, J., Tao, J., Xu, W., Kuang, Y., Wang, Q., Sun, Y., Zhou, G., Cheng, Y., and Su, H.: Exploring HONO formation and its role in driving secondary pollutants formation during winter in the North China Plain, J. Environ. Sci., 132, 83-97, https://doi.org/10.1016/j.jes.2022.09.034, 2023.